Supporting Figures

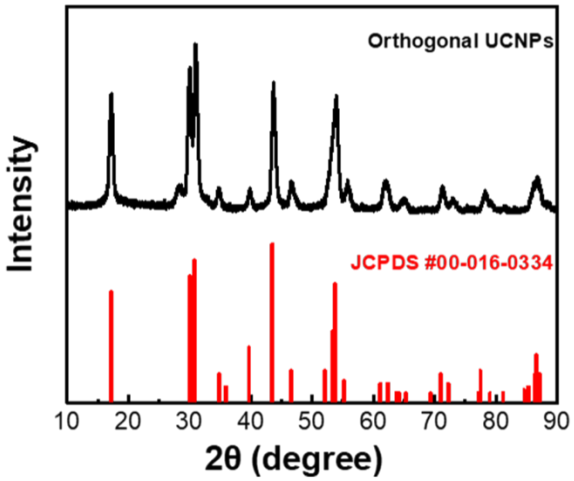

Figure S1. The XRD of orthogonal UCNPs.

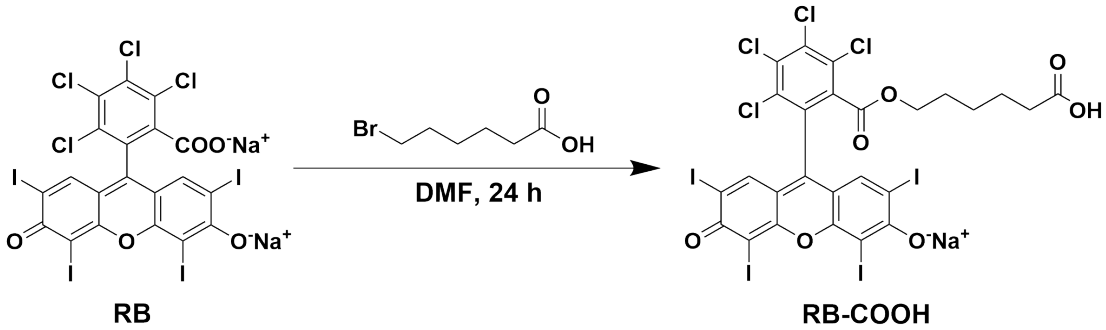

Figure S2. Synthetic scheme of RB-COOH.

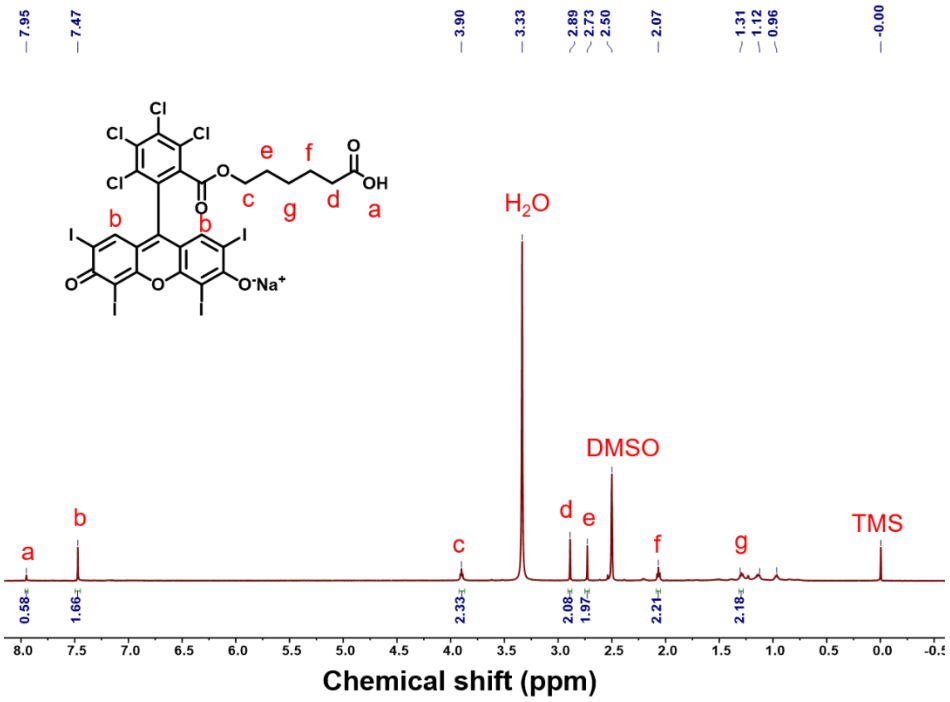

Figure S3. ^{1}H NMR spectra of RB-COOH.

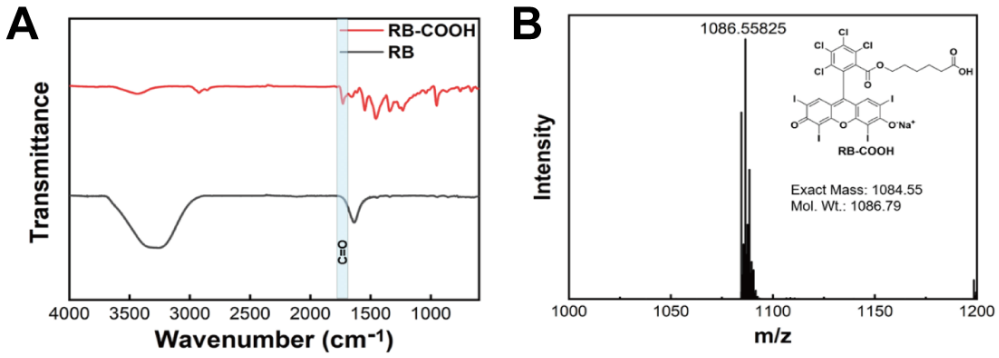

Figure S4. FT-IR (A) and HRMS mass spectrum (B) of RB-COOH.

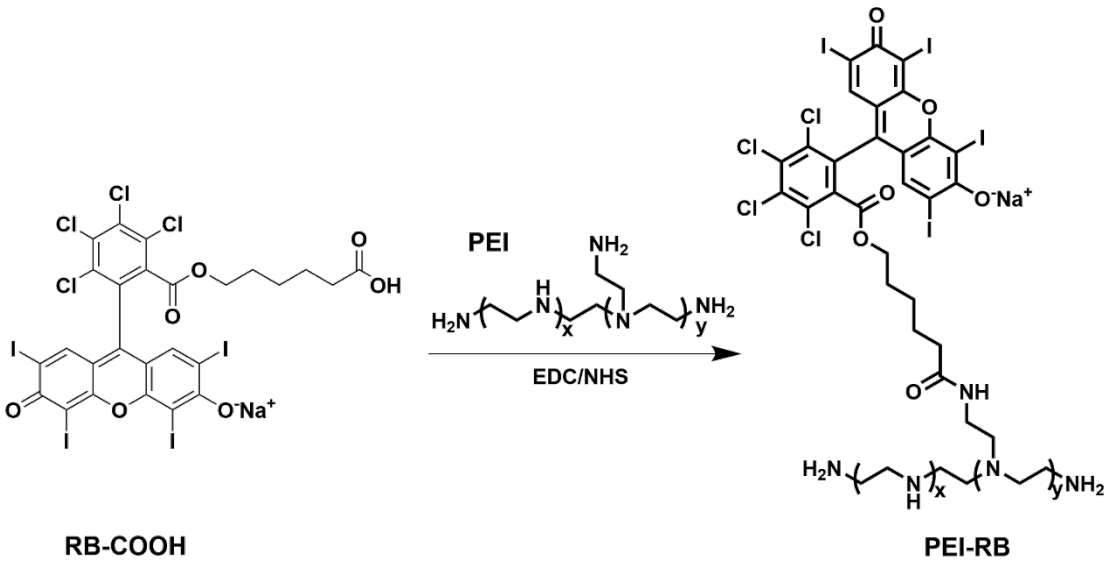

Figure S5. Synthetic scheme of PEI-RB.

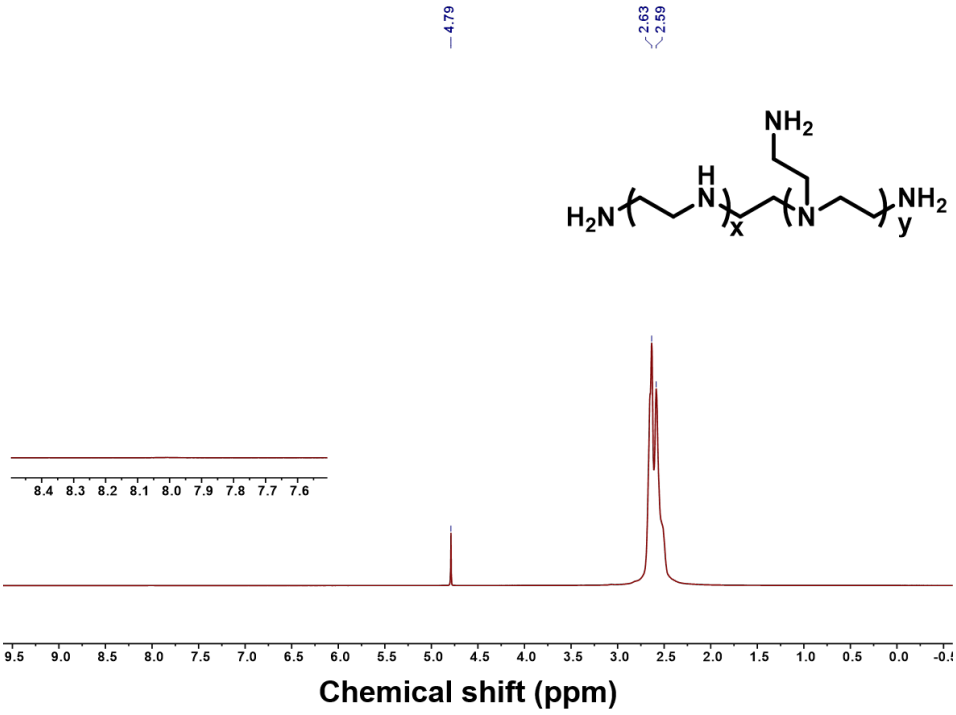

Figure S6. ^{1}H NMR spectra of PEI.

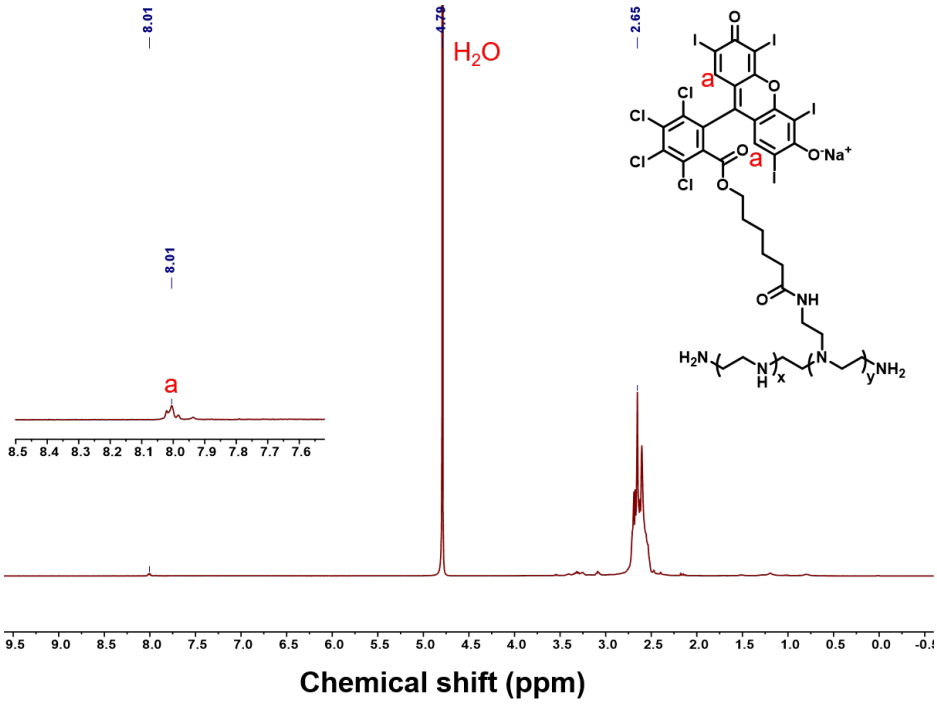

Figure S7. ^{1}H NMR spectra of PEI-RB.

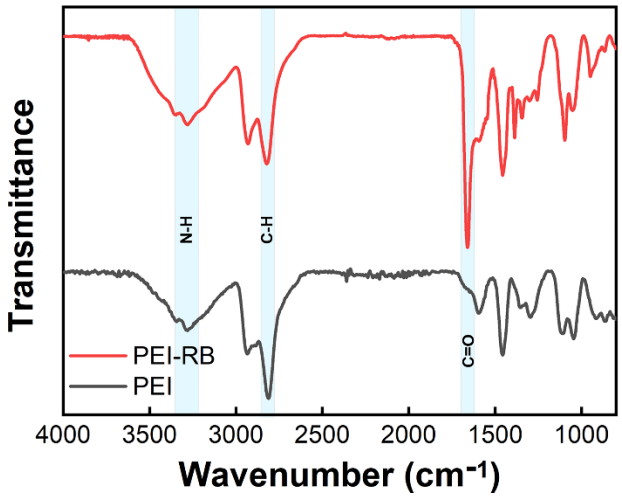

Figure S8. FT-IR of PEI and PEI-RB.

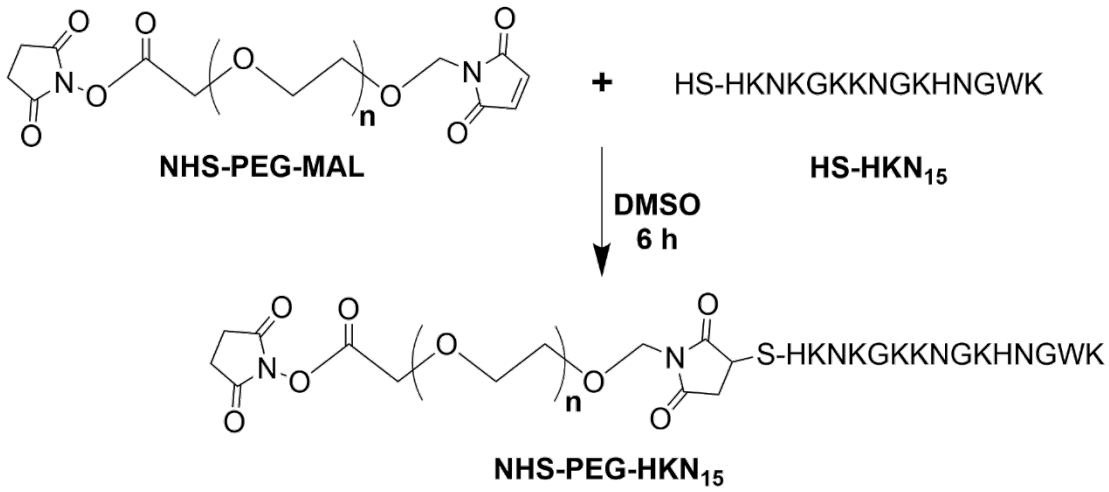

Figure S9. Synthetic scheme of NHS-PEG-HKN15.

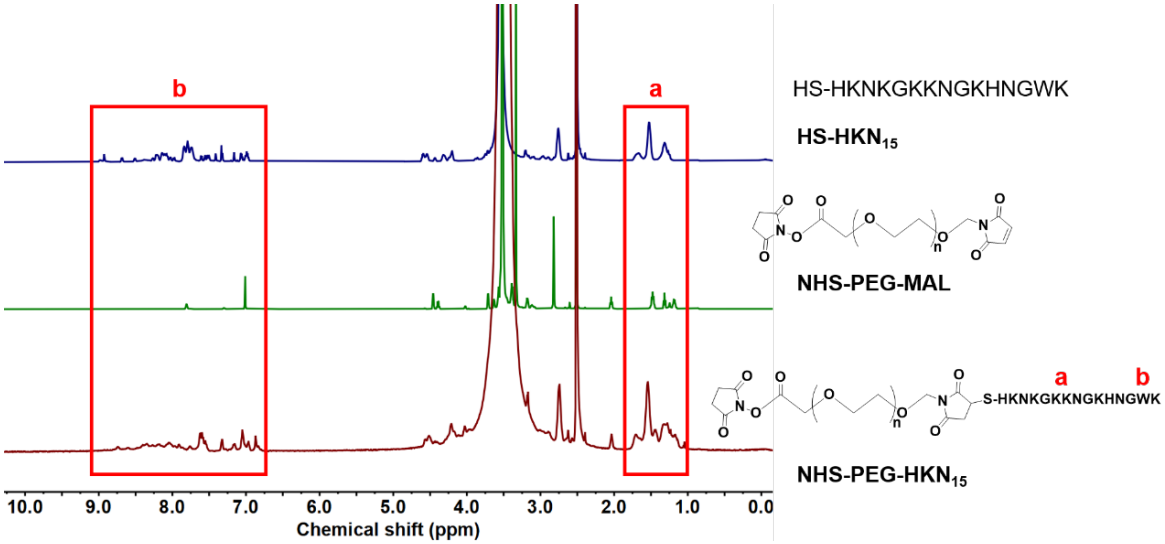

Figure S10. ^{1}H NMR spectra of HKN15, NHS-PEG-Mal, and NHS-PEG-HKN15.

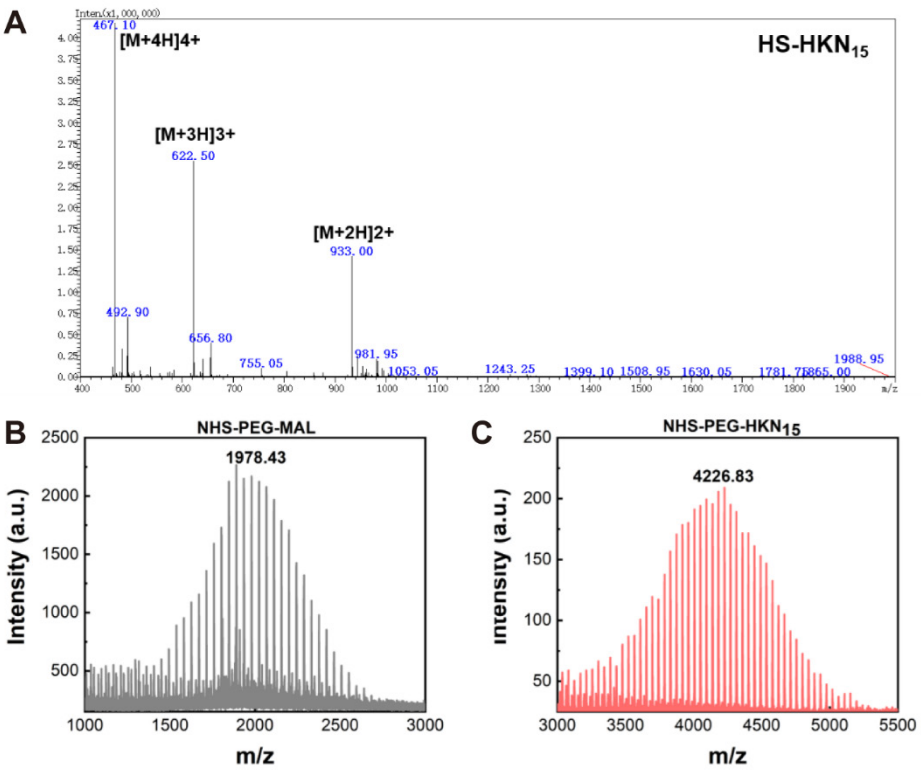

Figure S11. HRMS mass spectrum of (A) HKN_{15}, (B) NHS-PEG-Mal, and (C) NHS-PEG-HKN_{15}.

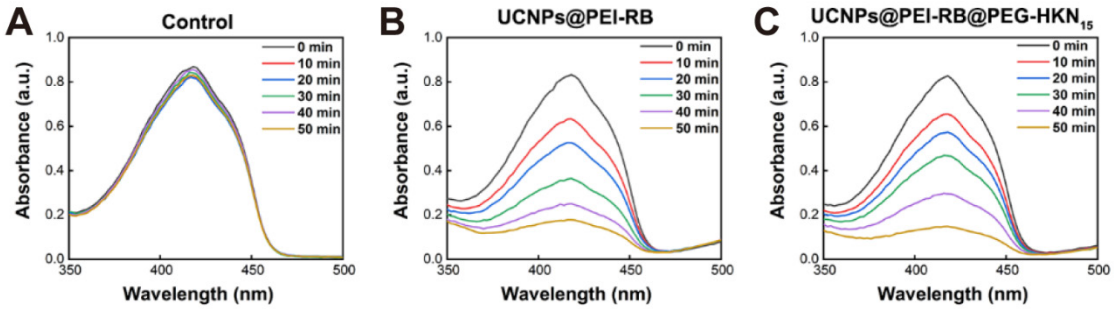

Figure S12. UV–vis assay of ROS generation using DPBF probe.

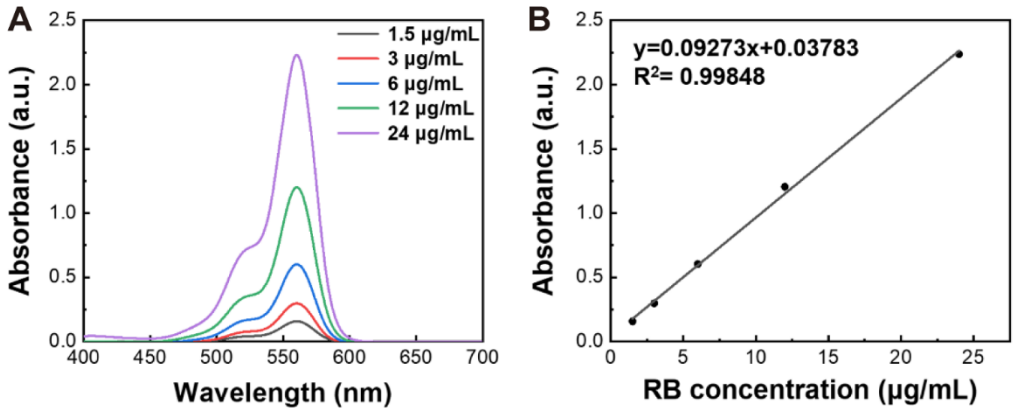

Figure S13. (A) UV-Vis absorption analysis and (B) the standard curve of RB

(absorbance at 560 nm).

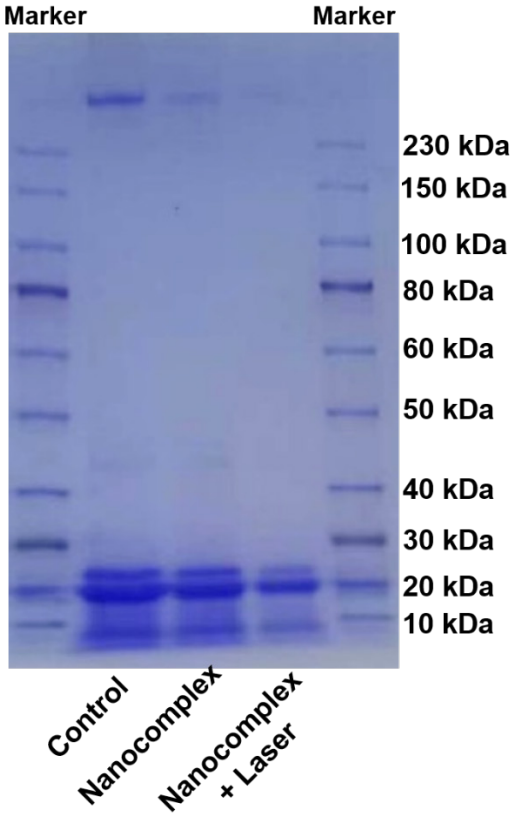

Figure S14. SDS-PAGE analysis of surface-functionalized UCNPs-induced ferritin degradation.

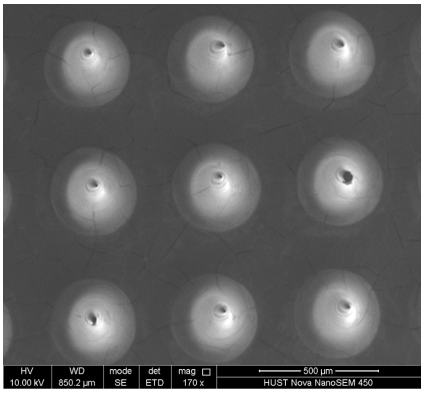

Figure S15. Scanning electron microscopy (SEM) images of OUSMNs.

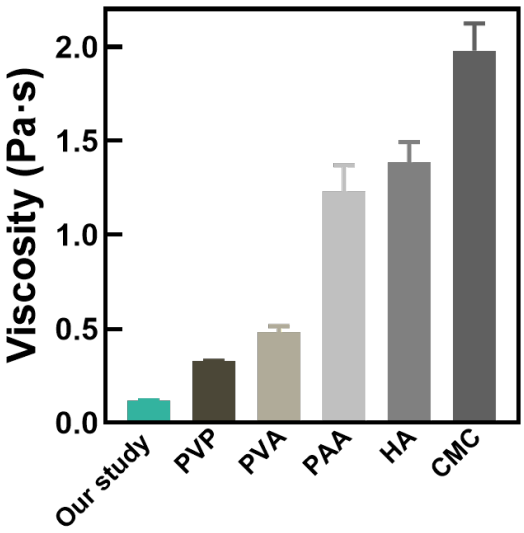

Figure S16. Comparison of matrix solution viscosity between OUSMNs and five commonly used polymer-based dissolving microneedles.

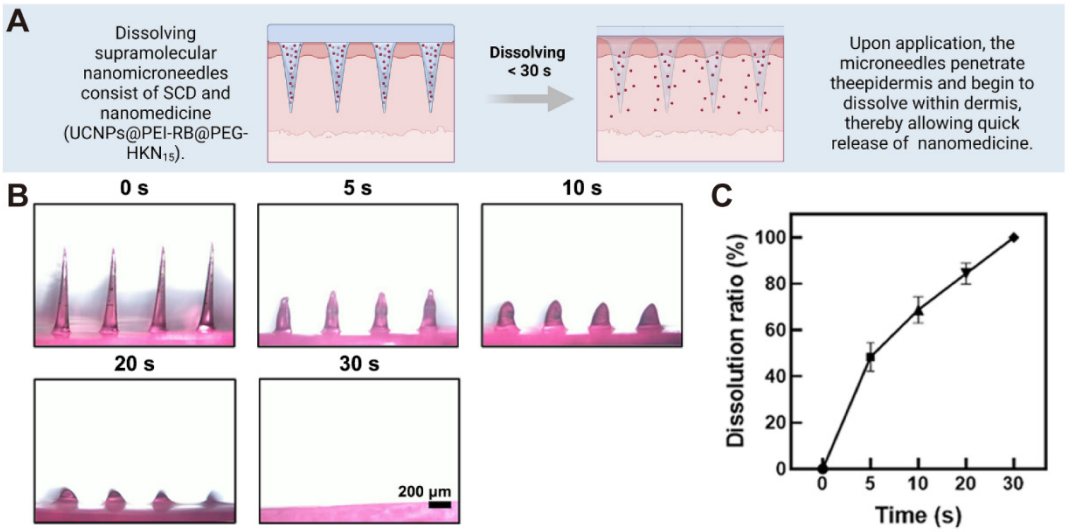

Figure S17. Dissolution rate of OUSMNs. (A) Diagram illustrating the dissolution mode of OUSMNs. (B) Dissolution of OUSMNs in a modified gelatin skin model over different durations. (C) Statistical chart of the dissolution rate of OUSMNs.

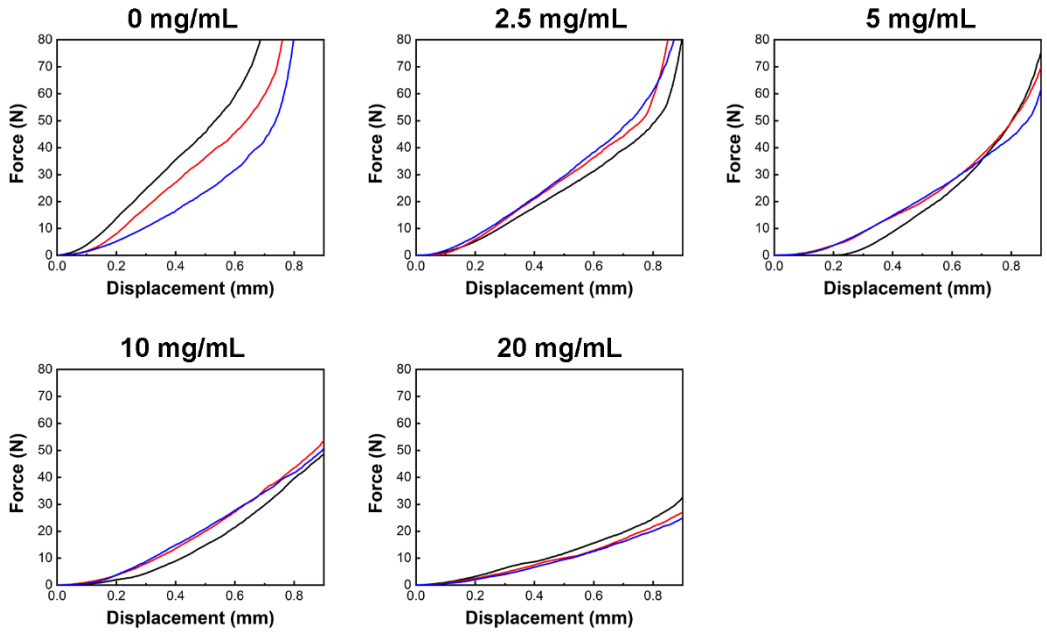

Figure S18. Comparison of compression force-displacement curves for various concentrations of OUSMNs.

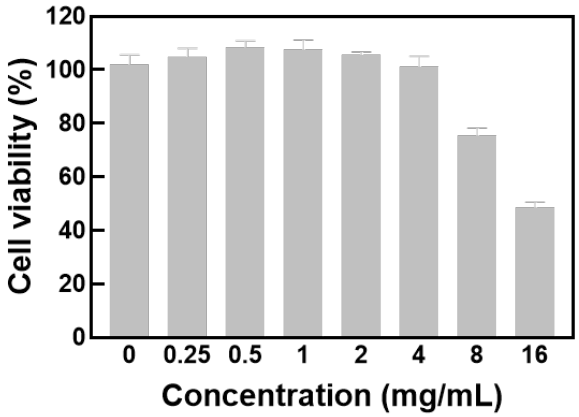

Figure S19. Biosafety evaluation of OUSMNs in KFs.

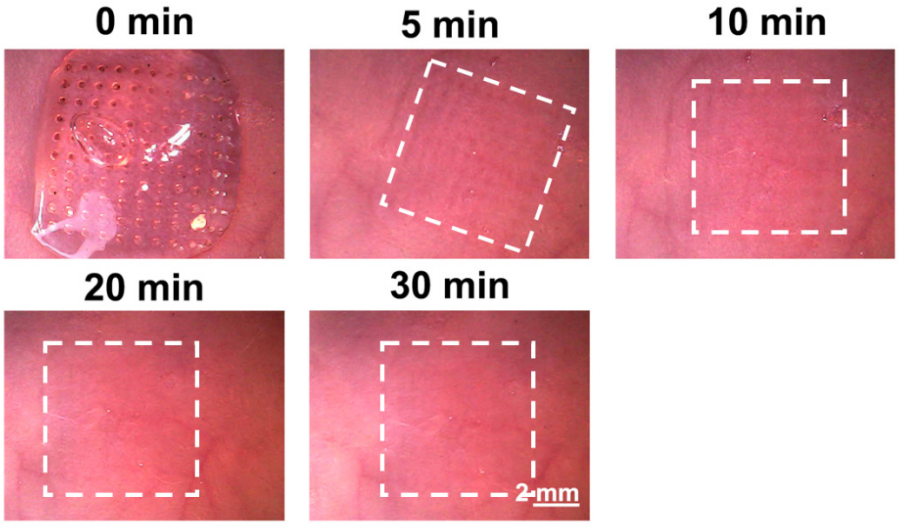

Figure S20. Skin recovery after application of OUSMNs.

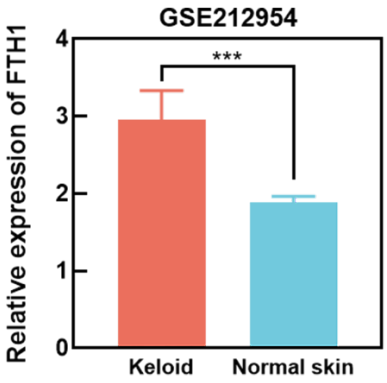

Figure S21. Bioinformatics analysis of ferritin (gene name: FTH1) gene expression levels in keloid tissues compared to normal skin tissues.

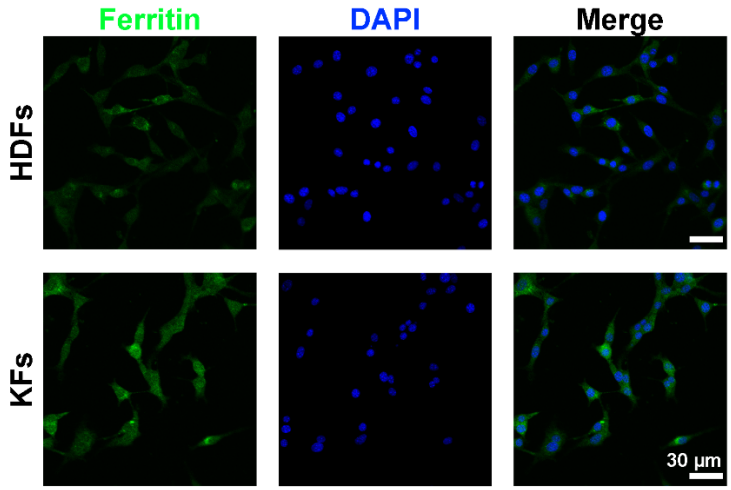

Figure S22. Immunofluorescence (IF) staining of ferritin in KFs and HDFs.

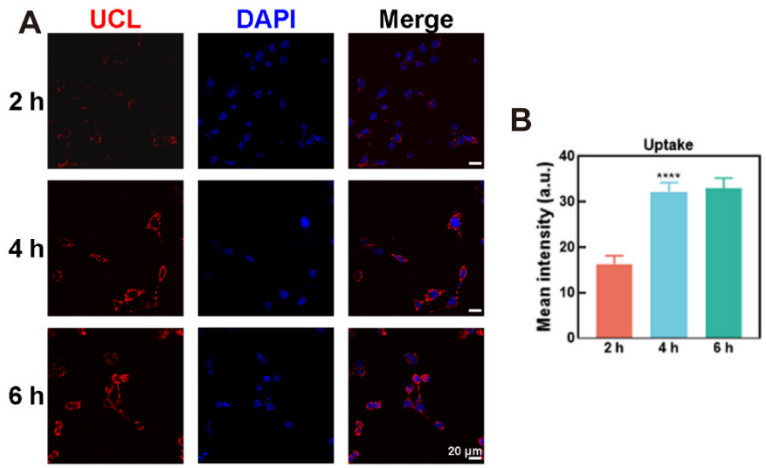

Figure S23. Evaluation of KFs uptake of OUSMNs using two-photon CLSM.

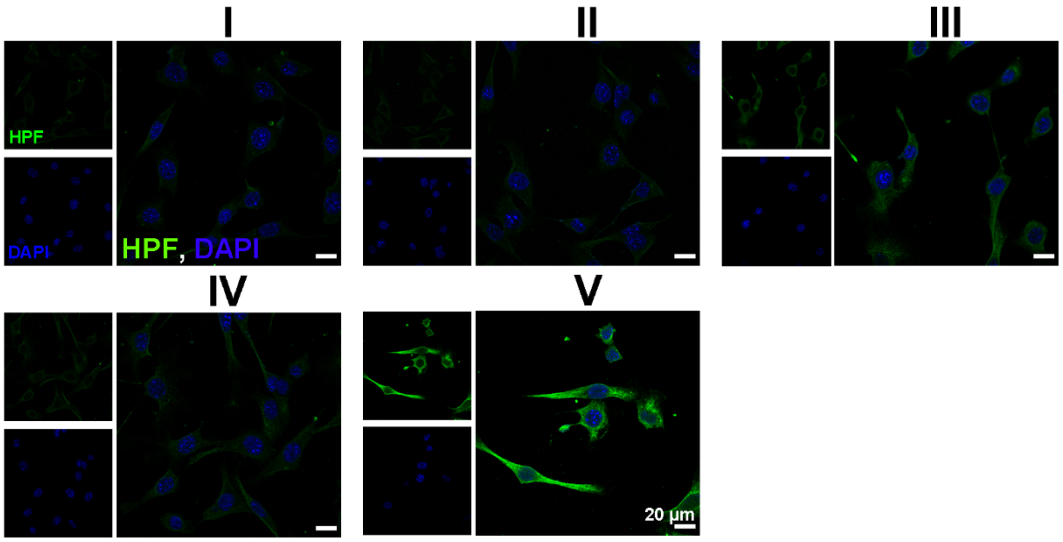

Figure S24. IF staining of HPF in KFs.

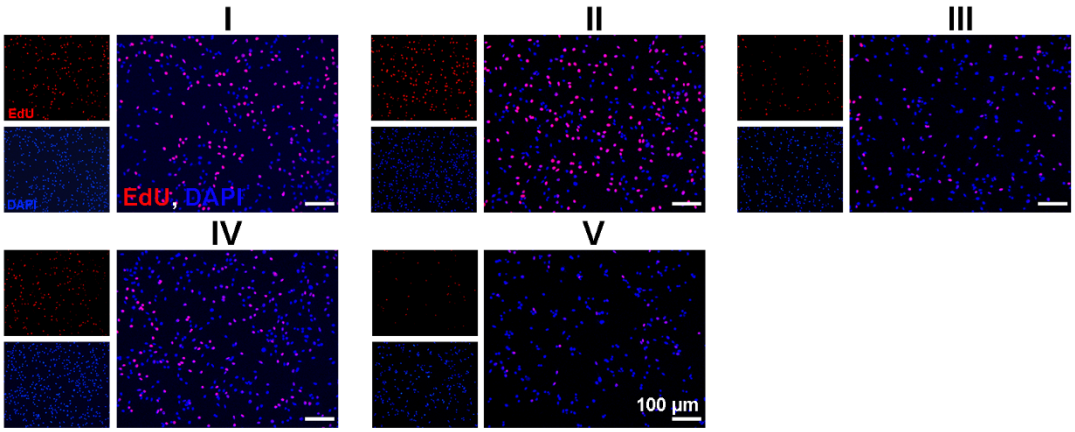

Figure S25. EdU staining was applied to assess cell proliferation, with EdU (red fluorescence) marking proliferating cells and DAPI (blue fluorescence) marking total

cells.

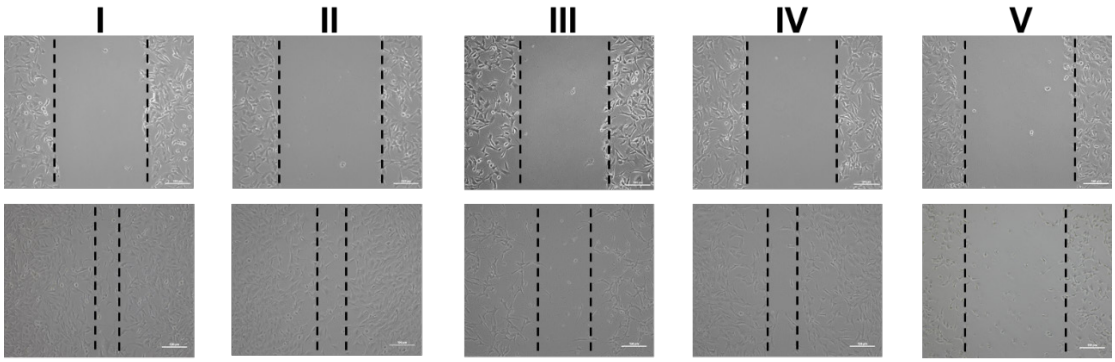

Figure S26. The cell scratch assay was used to evaluate cell migration capability. Scale bar=100 μm.

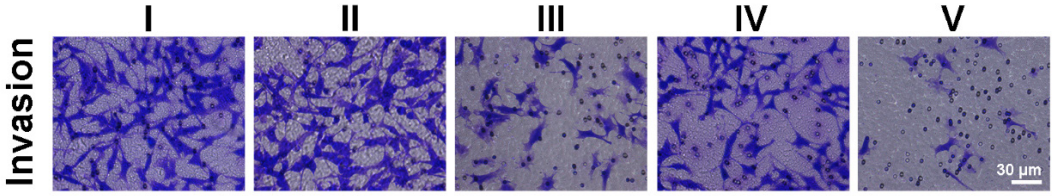

Figure S27. The Transwell invasion assay was used to evaluate cell invasive capacity.

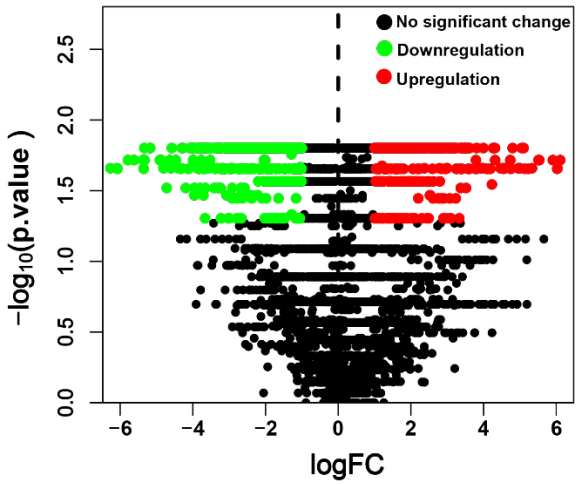

Figure S28. The volcano plot depicted differentially expressed genes.

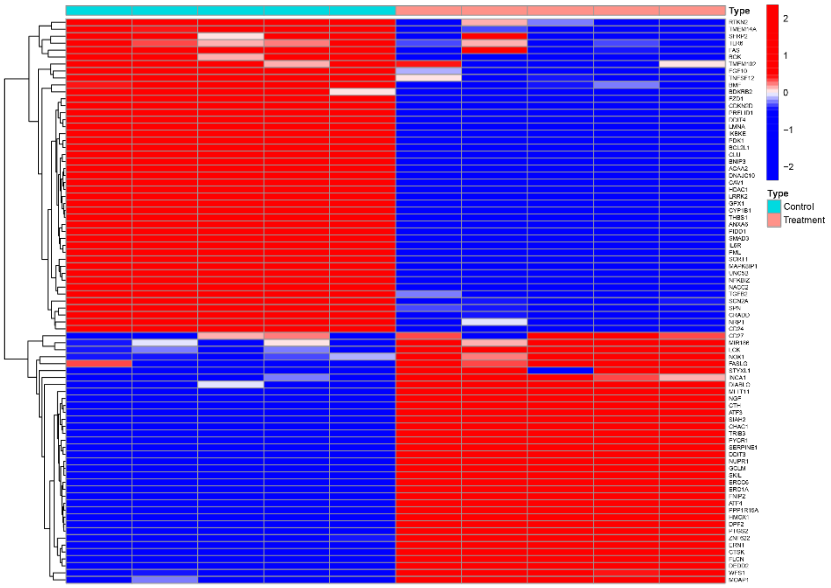

Figure S29. Heatmap of markers for cell apoptotic process selected from the mRNA sequencing data after OUSMNs treatment.

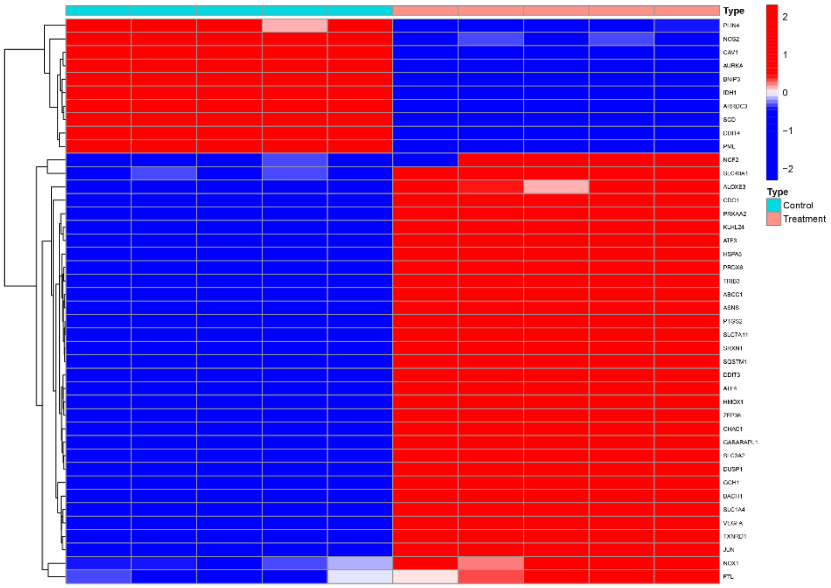

Figure S30. Heatmap of markers for ferroptosis selected from the mRNA sequencing data after OUSMNs treatment.

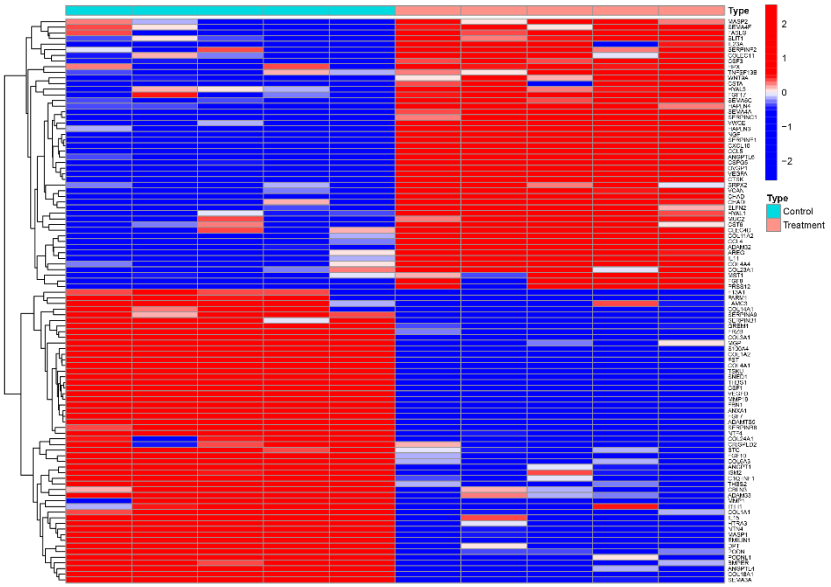

Figure S31. Heatmap of markers for extracellular matrix (ECM) deposition selected from the mRNA sequencing data after OUSMNs treatment.

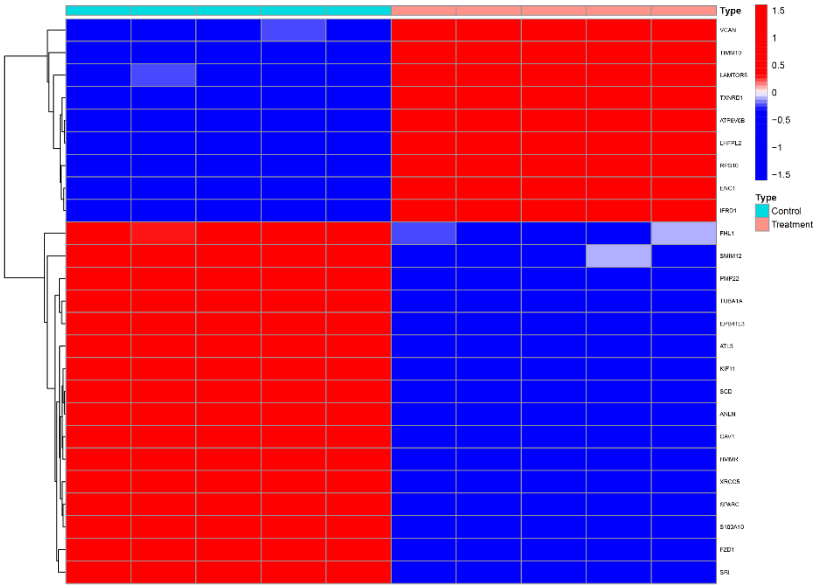

Figure S32. Heatmap of markers for epithelial-mesenchymal transition (EMT) process selected from the mRNA sequencing data after OUSMNs treatment.

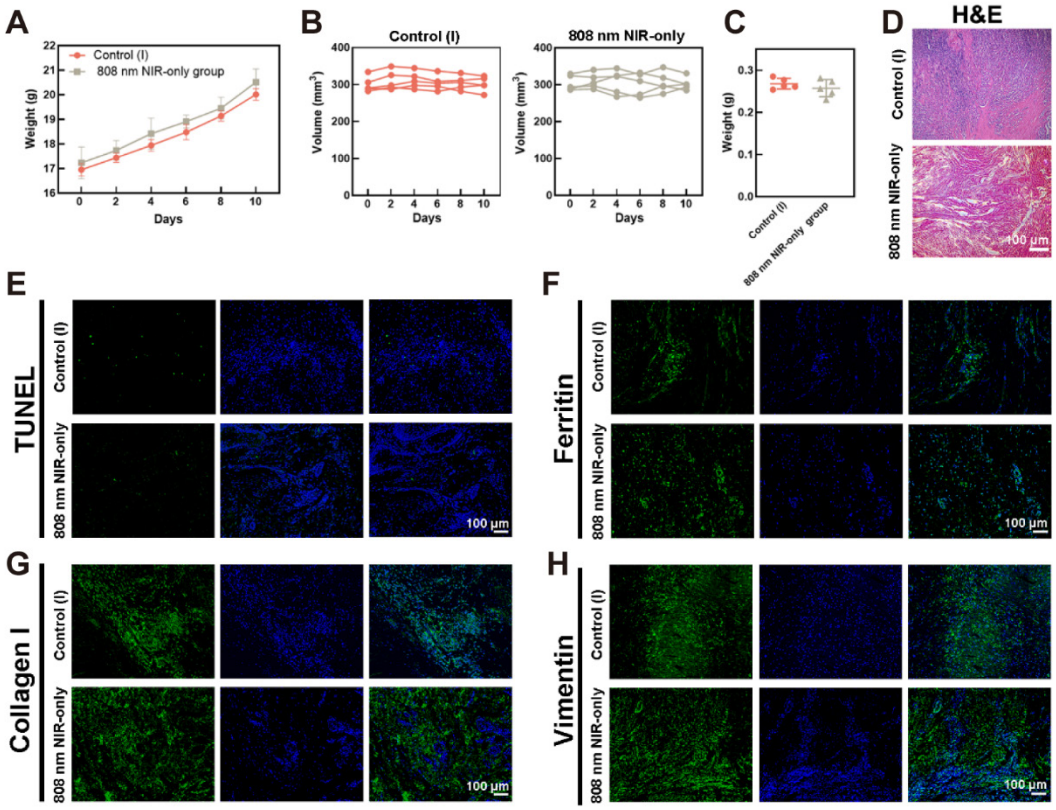

Figure S33. The effect of 808 nm NIR-only irradiation on a subcutaneous keloid xenograft model in nude mice. (A) Body weight variations in nude mice treated with NIR-only irradiation. (B) The growth curves of keloid transplantations in the control group and 808 nm NIR-only irradiation group. (C) Weight of keloid grafts in the control group and 808 nm NIR-only irradiation group. Histological observation of the keloid grafts with staining of (D) H&E, (E) TUNEL, (F) Ferritin, (G) Collagen I, and (H) Vimentin in the control group and 808 nm NIR-only irradiation group.

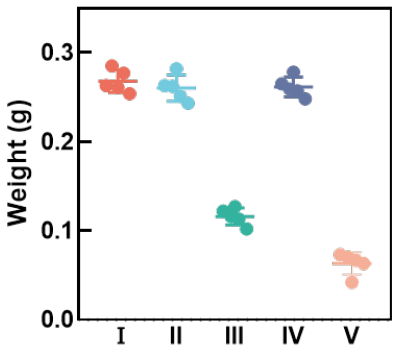

Figure S34. Weight of keloid grafts in groups I- IV.

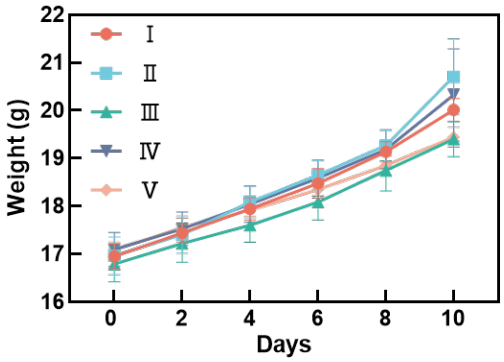

Figure S35. Body weight variations in nude mice treated with groups I- IV.

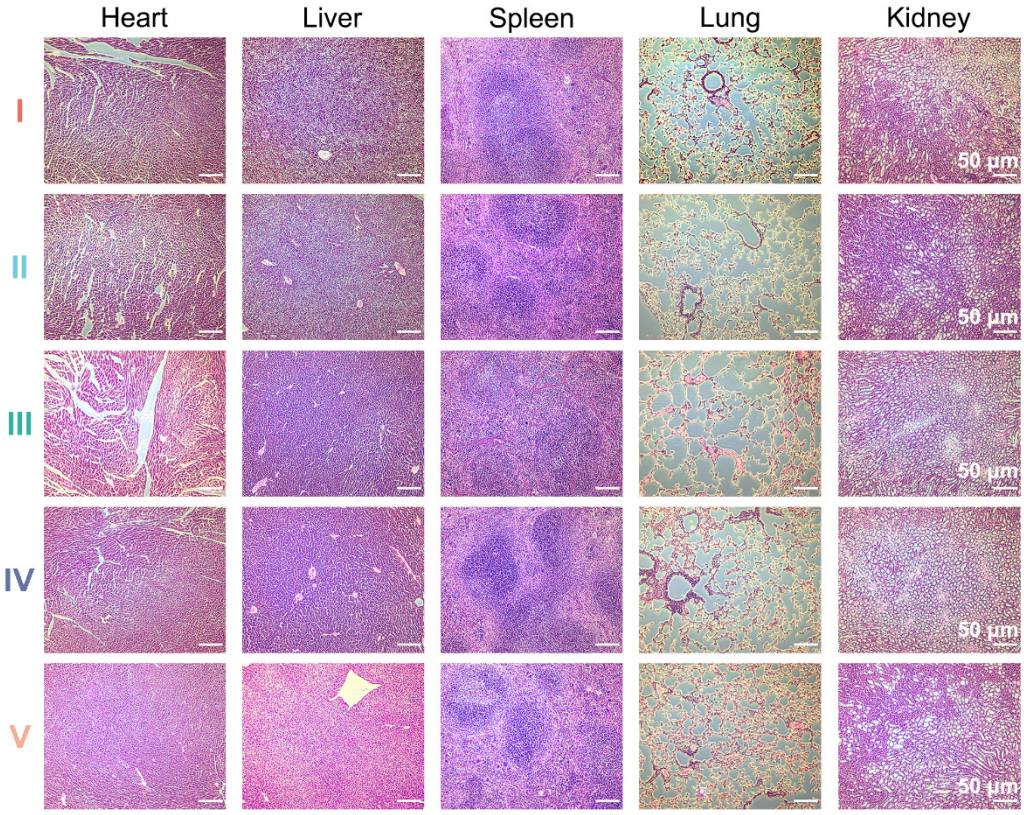

Figure S36. H&E-stained images of vital organs in nude mice with groups I- IV.

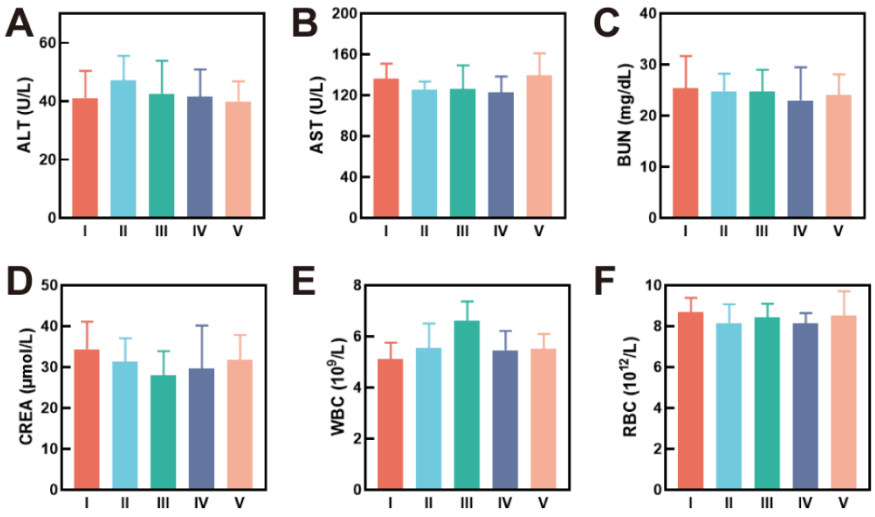

Figure S37. Assess the liver and kidney functions of nude mice treated with groups I-IV.

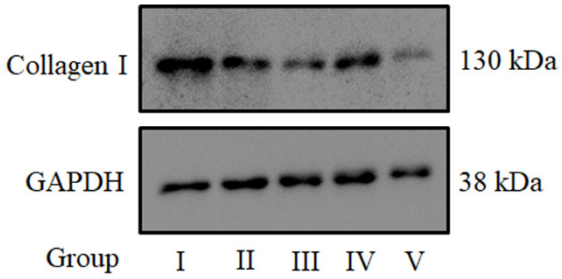

Figures S38. Western blot analysis was conducted to measure Collagen I expression protein level.